# Spontaneous adsorption of ions on graphene at the electrolyte-graphene interface

Cite as: Appl. Phys. Lett. 117, 203102 (2020); https://doi.org/10.1063/5.0023191 Submitted: 27 July 2020 . Accepted: 08 November 2020 . Published Online: 19 November 2020

🗓 Jianbo Sun, 🗓 Luca Camilli, 🗓 José M. Caridad, 🗓 Jaime E. Santos, and 🗓 Yuxin Liu







/iew Online



# Your Qubits. Measured.

Meet the next generation of quantum analyzers

- Readout for up to 64 qubits
- Operation at up to 8.5 GHz, mixer-calibration-free
- Signal optimization with minimal latency







# Spontaneous adsorption of ions on graphene at the electrolyte-graphene interface

Cite as: Appl. Phys. Lett. 117, 203102 (2020); doi: 10.1063/5.0023191 Submitted: 27 July 2020 · Accepted: 8 November 2020 · Published Online: 19 November 2020

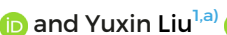














## **AFFILIATIONS**

Lane Department of Computer Science and Electrical Engineering, West Virginia University, Morgantown, West Virginia 26506, USA

#### **ABSTRACT**

We report the spontaneous adsorption of ions on graphene at the interface with electrolytes through an investigation based on the electrolyte-gated field effect transistor configuration. It is found that the gate voltage at which the minimum conductivity occurs in these devices is highly sensitive to the type of ions and their concentrations in the electrolytes; yet the experimental results exhibit non-trivial deviations from the predictions based on the Gouy-Chapman-Stern (GCS) model, which only takes account of the electrostatic interactions among the charges in the system. By incorporating a Langmuir-type adsorption term into the GCS model, we achieve quantitative alignment with the experiments, thus demonstrating that these deviations originate from the spontaneous adsorption of ions onto graphene. Analysis of the transport characteristics in these devices indeed confirms the existence of the adsorbed ions.

Published under license by AIP Publishing. https://doi.org/10.1063/5.0023191

The interface between solid and liquid is a topic of great scientific and technological importance. In the specific case of graphene and aqueous medium, for instance, it plays a critical role in many emerging applications of graphene, e.g., analytical chemistry,2 energy storage and conversion,3 water filtration,4 and biosensing.5 Unraveling the behavior at the interface is especially important for graphene because, being a one-atom-layer material, its physical properties are highly sensitive to the surrounding environment.<sup>6-9</sup> In addition, the unique atomic structure of graphene with highly delocalized  $\pi$ -orbitals could give rise to various interfacial behaviors, for instance, doping-tunable wettability<sup>10</sup> and frictionless water transport.<sup>11</sup> Past studies revealed varying effects at the electrolyte-graphene interface, and such effects were shown to be strongly dependent on the type of ions and their concentrations, which points to the importance of the presence of mobile ions in the electrolytes. 12

In this context, relevant studies have been performed through an electrolyte-gated field effect transistor (EGFET) configuration, from which the carrier transport properties of graphene and the interfacial capacitance can be obtained. 13,14,16-18 Mathematical models were also proposed for the electrolytically gated graphene, from which the

sensitivity of the doping level in graphene to the salt concentration was demonstrated. However, in these studies only the electrostatic interactions between the charges in the system were considered; while other mechanisms, such as adsorption of ions on graphene, were neglected. 18,19 This is in contrast to recent first-principles calculations and molecular dynamics simulations pointing out that even the most common ions, such as  $H_3O^+$ ,  $OH^-$ ,  $K^+$ , and  $Cl^-$ , can exhibit strong affinity toward the graphene surface. Such ion-adsorption behavior is attributed to a variety of mechanisms, including the loss of the ions' solvation shells, 22,23 donor-acceptor interaction, 21 induced dipole-dipole interaction,<sup>23</sup> surface-induced water structure,<sup>22</sup> etc. Experimental evidence indicating the accumulation of ions on graphene via in situ Raman spectroscopy, <sup>17</sup> deep UV second harmonic generation measurements,<sup>27</sup> or atomic force microscopy,<sup>28</sup> was also reported. The ions adsorbed on graphene may alter graphene's surface potential and affect its carrier transport; yet in currently existing studies based on the EGFET configuration, the adsorption of ions on graphene has not been unveiled.

In this paper, we report the observation of spontaneous ion adsorption on graphene in the EGFET by measuring its electrical

<sup>&</sup>lt;sup>2</sup>Department of Physics, Technical University of Denmark, 2800 Kgs. Lyngby, Denmark

<sup>&</sup>lt;sup>3</sup>Dipartimento di Fisica, Università degli studi di Roma "Tor Vergata," 00133 Roma, Italy

<sup>&</sup>lt;sup>4</sup>Centro de Física, Universidade do Minho, P-4710-057 Braga, Portugal

<sup>&</sup>lt;sup>5</sup>Instituto de Polímeros e Compósitos, Universidade do Minho, P-4800-058 Guimarães, Portugal

<sup>&</sup>lt;sup>a)</sup>Author to whom correspondence should be addressed: yuxin.liu@mail.wvu.edu

characteristics upon exposure to electrolytes with different types of ions and concentrations. Figure 1(a) shows a representative device in which a polydimethylsiloxane (PDMS) well is applied as the container for the electrolytes, and a standard Ag/AgCl reference electrode is employed as the gate electrode. An enlarged view of the graphene channel is displayed in Fig. 1(b) with the metal electrodes (source and drain) being passivated by a photoresist layer. The single-layer nature and the structural integrity of the graphene channel are verified by the characteristic Raman spectrum as shown in Fig. 1(c). We measured the electrical responses of the devices loaded with different electrolytes, KCl, NaCl, or HCl, at varying concentrations. These electrolytes were chosen because they are commonly found in physiological and water environments. The details about device fabrication, Raman spectroscopy, and electrical measurements are given in the supplementary material.

Figures 2(a)-2(c) display the  $I_d - V_g$  curves of a typical EGFET device that was loaded with NaCl, KCl, and HCl solutions at varying concentrations, respectively. As is shown, all  $I_d - V_g$  curves exhibit ambipolar behavior, which is attributed to the semimetal band structure of graphene with the conduction band and the valence band meeting at the Dirac point with linear dispersion. The minimum conductivity occurs at the charge neutrality point (CNP), and the corresponding gate voltage is defined as  $V_{CNP}$ . Our devices consistently show p-type behavior, which could be due to the negatively charged impurities on the substrates,<sup>29</sup> p-doping effect of water molecules<sup>30</sup> as well as adventitious contaminations, or a combination of those effects. The most prominent impact of the electrolytes on the EGFET is the horizontal shift of the  $I_d - V_g$  curves as the electrolytes' concentration changes. As reported in Figs. 2(a) and 2(b), the  $I_d - V_g$ curves shift toward negative gate voltage as the concentrations of NaCl and KCl increase; however, such a shift reverses its direction in HCl at the concentration of  $\sim 0.05$  M [Fig. 2(c)]. The extracted  $V_{CNP}$  values from the  $I_d - V_g$  curves are plotted in Fig. 2(d), in which the nonmonotonous shift of  $V_{CNP}$  in HCl is clearly illustrated.

The downward shift of  $V_{CNP}$  as the electrolyte concentration increases has been observed in previous studies,  $^{13,16,17}$  and it is normally attributed to the increased gate capacitance in electrolytes at higher concentrations.  $^{13,16,17,19,20}$  Mišković *et al.*  $^{18-20}$  derived a series

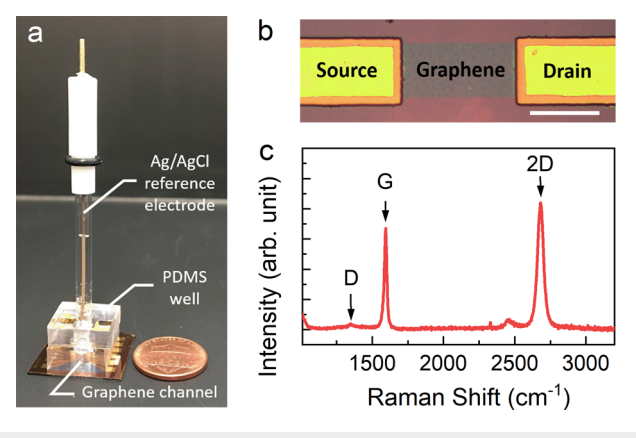


**FIG. 1.** (a) Photo showing a typical EGFET device; (b) enlarged view of the graphene channel (scale bar: 100  $\mu$ m); and (c) typical Raman spectrum collected from the graphene channel.

of models for the electrolytically gated graphene in the framework of the Gouy–Chapman–Stern (GCS) theory using the Poisson–Boltzmann (PB) equation. In these models, the electrolyte–graphene interface is defined as an electrical double layer (EDL) with a diffuse layer that is separated from graphene by a charge-free Stern layer. <sup>18–20</sup> For the sake of brevity, in the following equations,  $\beta \equiv \frac{1}{(k_BT)}$ , with  $k_B$  being the Boltzmann constant and T being the temperature (assumed to be 300 K). The charge distribution across the interface satisfies the charge neutrality condition: <sup>19,20</sup>

$$\sigma_{imp} + \sigma_{gr} + \sigma_{dl} = 0, \tag{1}$$

where  $\sigma_{imp}$  is the effective impurity charge density on SiO<sub>2</sub>,  $\sigma_{gr}$  is the net charge carrier density in graphene, and  $\sigma_{dl}$  is the charge density in the diffuse layer due to the redistribution of ions driven by the applied gate voltage.  $\sigma_{dl}$  is a function of the potential drop across the diffuse layer  $(V_{dl})$ , <sup>1,31</sup>

$$\sigma_{dl} = 4zec_0\lambda_D \sinh\left(\frac{ze\beta V_{dl}}{2}\right),$$
 (2)

for a symmetric z: z electrolyte of concentration  $c_0$ , with e being the charge of a proton. In Eq. (2),  $\lambda_D$  is the Debye screening length given by<sup>1,31</sup>

$$\lambda_D = \sqrt{\frac{\varepsilon_w \varepsilon_0}{2z^2 e^2 c_0 \beta}},\tag{3}$$

with  $\varepsilon_w$  being the dielectric constant of water and  $\varepsilon_0$  being the vacuum permittivity. By using the low-energy approximation of the density of states for graphene's  $\pi$ -electron band,  $\mathcal{D}(\epsilon) = \frac{2|\epsilon|}{\pi(\hbar \nu_F)^2}$ , where  $\nu_F \approx 10^6$  m/s is the Fermi velocity of graphene, and letting  $V_0 \equiv (\epsilon_F - \overline{\epsilon}_D)/e$  be the average electrostatic potential in graphene, the charge carrier density in graphene can be calculated as  $^{32}$ 

$$\sigma_{gr}(V_0) = \frac{2e}{\pi} \left(\frac{1}{\hbar \nu_F \beta}\right)^2 \left\{ \text{dilog} \left(1 + e^{e\beta V_0}\right) - \text{dilog} \left(1 + e^{-e\beta V_0}\right) \right\},\tag{4}$$

with dilog being the standard dilogarithm function. The Stern layer can be considered as a plate capacitor with thickness h and the potential drop across it ( $V_{stern}$ ) can be estimated as  $^{19,20}$ 

$$V_{stern} = \frac{4\pi h \sigma_{dl}}{\varepsilon_{cur^{c_0}}},\tag{5}$$

in which  $\varepsilon_{\rm sw}$  is the reduced dielectric constant of water due to the dielectric saturation in a high electrical field. Combining Eqs. (1)–(5), we can derive the potential distribution in the system with an applied gate voltage  $V_g$  being  $^{18-20}$ 

$$V_g = V_0 + V_{stern} + V_{dl} + V_{fb}, (6)$$

in which  $V_{dl}$  is the potential drop across the diffuse layer;  $V_{fb}$  is the flatband voltage that compensates the different work functions of each component in the system, which would give a constant offset of the measured  $V_{CNP}$ .

At  $V_g = V_{CNP}$ , the gate-induced charge carrier density in graphene vanishes, i.e.,  $\sigma_{gr} = 0$ . By solving Eqs. (1)–(6), we can calculate the  $V_{CNP}$  of the system with a charge impurity density  $\sigma_{imp}$  at different

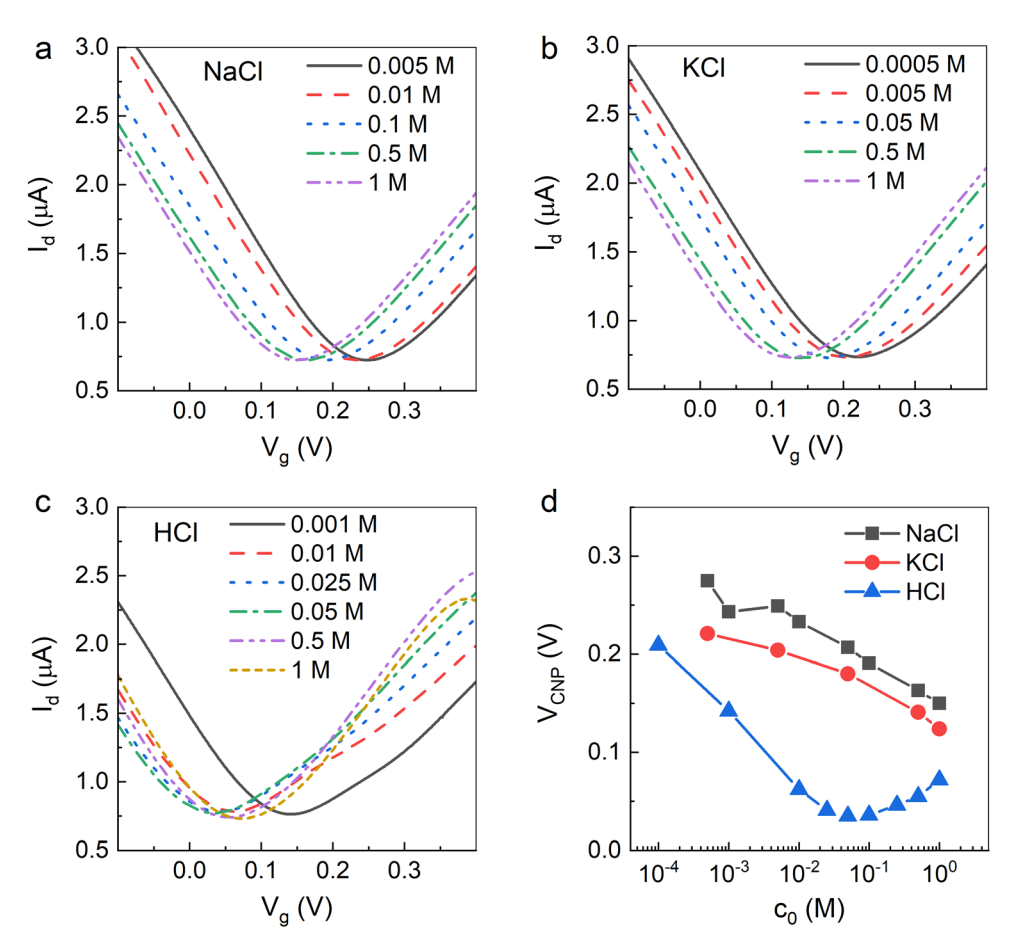


FIG. 2.  $I_d - V_g$  curves measured from a typical EGFET device loaded with (a) NaCl, (b) KCl, and (c) HCl at different concentrations; (d)  $V_{CNP}$  as a function of the electrolyte concentration extracted from the  $I_d - V_g$  curves in (a) to (c).

ion concentrations. The standard set of parameters are  $h=0.3\,\mathrm{nm}$ , z=1,  $\varepsilon_w=80$ , and  $\varepsilon_{sw}=10.^{18-20,33}$  The calculated  $V_{CNP}$  values as a function of the electrolytes' concentration are plotted as the dashed lines in Fig. 3(a), along with the experimental data that are amended with the liquid junction potential. As shown in the figure, for KCl and NaCl, the calculated results show an overall downward trend of  $V_{CNP}$  as  $c_0$  increases, similar to the experimental results; yet some differences can be clearly observed. On the other hand, the calculated results fail to replicate the non-monotonous behavior of  $V_{CNP}$  for HCl. Such discrepancies between theory and experiment suggest that additional mechanisms, other than the electrostatic effect described by the PB equation, should be considered when describing the electrolyte/graphene interface.

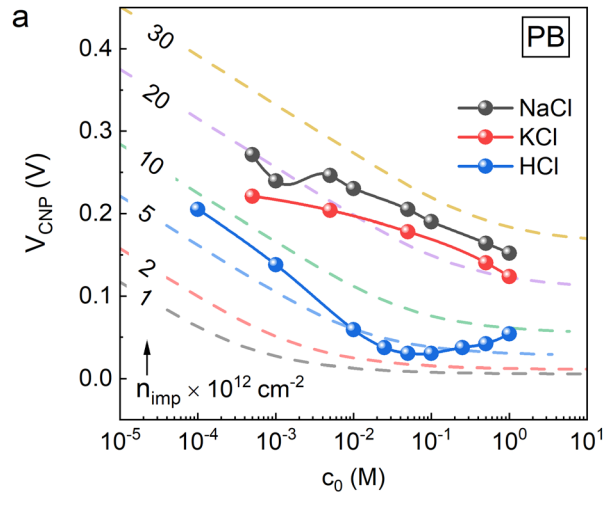
As mentioned previously, one of the possible mechanisms that have been neglected so far but could play an important role is the specific adsorption of ions on graphene. To include such an effect, we introduce an adsorbed charged density  $\sigma_{ads}$  as described by the Langmuir adsorption isotherm,

$$\sigma_{ads} = sgn(\sigma_{ads}) \cdot e \cdot n_{ads}^{sat} \frac{c_0}{c_0 + K_D}, \tag{7}$$

with  $sgn(\sigma_{ads})$  and  $n_{ads}^{sat}$  being the sign and the saturation density of the dominating adsorbed ions on graphene, respectively, and  $K_D$  the reciprocal of the Langmuir constant. Here, we choose the Langmuir adsorption isotherm instead of others because it applies to the conditions of ion adsorption on graphene, such as monolayer adsorption, finite number of adsorption sites, and no significant positive/negative cooperative effect between different sites. With the adsorption term, the new charge neutrality condition in the system can now be described as

$$\sigma_{dl} + \sigma_{gr} + \sigma_{imp} + \sigma_{ads} = 0.$$
 (8)

Combining Eqs. (2)–(8), we recalculated the  $V_{CNP}$  of the system as a function of  $c_0$ . The calculated  $V_{CNP}$ , with  $n_{ads}^{sat} = 5 \times 10^{13}$  cm<sup>-2</sup>, which is estimated with an ion–ion separation of the Bjerrum length considering the dielectric saturation of water at the interface, <sup>31</sup> and  $K_D = 0.05$  M are plotted as the blue dashed line in Fig. 3(b). The calculation of  $n_{ads}^{sat}$  can be found in the supplementary material. The other factor,  $sgn(\sigma_{ads})$ , is determined by how the experimental results deviate from the predictions of the PB equation in Fig. 3(a). For example, for KCl and NaCl, the experimental plots exhibit a smaller slope than the theoretical predictions, suggesting that negatively charged ions are added to the negative charged impurities on the substrates, and



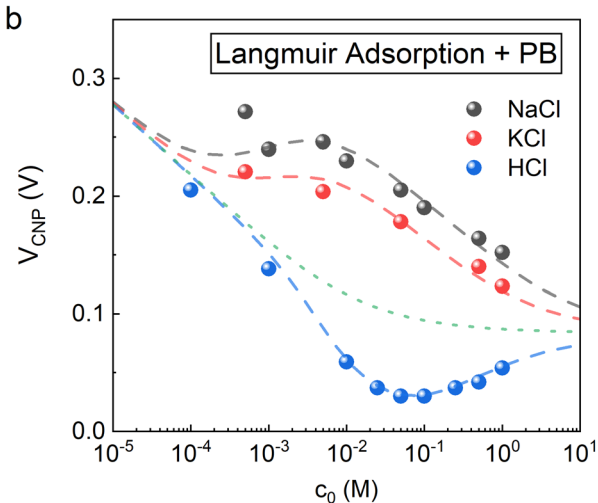


**FIG. 3.** (a) The measured  $V_{CNP}$  as a function of the electrolyte concentration (solid dots) and the predictions based on the PB equation with different charged impurity densities  $n_{imp}$  on  $\mathrm{SiO}_2$  (dashed lines). (b) The measured  $V_{CNP}$  as a function of the electrolyte concentration (solid dots) and the predictions based on the PB equation incorporated with the Langmuir adsorption isotherm (dashed lines). For comparison, the prediction based on the PB equation without taking account of ion adsorption is plotted as the green dotted line in (b).

thus  $sgn(\sigma_{ads})$  is negative. For HCl, the opposite applies. As shown in Fig. 3(b), accounting for a reasonable charge impurity density  $n_{imp} = 5 \times 10^{12} \, \text{cm}^{-2}$  and an accumulated  $V_{fb}$  of 0.06 V, with a positive  $sgn(\sigma_{ads})$ , the calculated results reproduce nicely the experimental data for HCl, strongly suggesting the specific adsorption of  $H_3O^+$  on graphene to be the origin of the observed reversion of the  $V_{CNP}$  shift for HCl. In other words, when the adsorbed  $H_3O^+$  overwhelms the negatively charged impurities on SiO<sub>2</sub>, the overall "impurity" charge density on graphene becomes positive and  $V_{CNP}$  shifts upwards upon further increasing the electrolyte concentration. By changing  $sgn(\sigma_{ads})$  to be negative, with the same  $n_{imp}$  and  $K_D = 0.004$  M, our model can also well replicate the experimental results for KCl [see the red dashed line in Fig. 3(b)]. Furthermore, a quantitatively accurate prediction of

the results for NaCl can also be achieved when  $V_{fb}$  is slightly increased by  $\sim 0.02 \,\mathrm{V}$  [black dashed line in Fig. 3(b)]. The good alignment of the above results indicates that Cl<sup>-</sup> adsorbs on graphene in KCl and NaCl, which adds to the negatively charged impurities on SiO<sub>2</sub> and leads to the up-lifted  $V_{CNP}$  relative to the theoretically calculated trend without taking account of ion adsorption [green dotted line in Fig. 3(b)].

The main parameters in the calculations above are summarized in Table I. A critical parameter is  $K_D$ , which is related to the adsorption energy that can be estimated by the Gibbs free energy change as  $\Delta G_{ad} = RT \ln K_D$ , with R being the gas constant. For  $K_D = 0.004$  M in NaCl and KCl,  $\Delta G_{ad} \approx -14\,\mathrm{kJ/mol}$ , which is close to the value (-20 kJ/mol) of the adsorption energy of Cl on electron-depleted (p-type) graphene calculated using the density function theory (DFT).<sup>21</sup> Such strong adsorption of these halide anions on electrondepleted graphene is attributed to the effective donor-acceptor interaction between them.<sup>21</sup> The higher  $\Delta G_{ad}$  value obtained by the DFT calculation could be because the DFT calculation is performed in a vacuum condition, which normally gives a higher adsorption energy.<sup>21,23</sup> In addition, the DFT calculations are limited by the finite size of the graphene sheet, which could deviate from the behavior of an "infinite" sheet due to the formation of the quadrupole moment in close proximity to ions. 35,36 For the case of HCl, as discussed above, our result suggests that H<sub>3</sub>O<sup>+</sup> exhibits a stronger adsorption on graphene than Cl-, which is in agreement with the higher adsorption energy of H<sub>3</sub>O<sup>+</sup> on graphene as obtained from DFT calculations.<sup>3</sup> Our results are also consistent with a recent molecular dynamics simulation of the ion density profile at the electrolyte-graphene interface, which shows that (1) in NaCl, only Cl- shows strong adsorption and (2) in HCl, both H<sub>3</sub>O<sup>+</sup> and Cl<sup>-</sup> are adsorbed, with H<sub>3</sub>O<sup>+</sup> adsorbing closer to graphene surface and at a higher concentration than Cl<sup>-</sup>. The strong adsorption of H<sub>3</sub>O<sup>+</sup> on graphene is most likely due to the amphiphilic nature of H<sub>3</sub>O<sup>+</sup> and the favorable interactions between the surface-induced electrical potential gradient and the permanent and induced dipoles of the ions.<sup>22</sup> In the Langmuir model, the stronger adsorption of  $H_3O^+$  implies a smaller  $K_D$  for  $H_3O^+$ , which seems to be in contradiction with the higher value of  $K_D$  used for HCl (0.05 M), compared with that used for NaCl and KCl (0.004 M). Nevertheless, this apparent contradiction is due to the fact that the Langmuir model only considers one species adsorbing on a surface, while in HCl, as described above, we have a more complicated system, with two ions interacting and adsorbing on graphene. In this sense, the  $K_D$  in our model is, in fact, an effective parameter that takes into account the adsorption of both cations and anions in the electrolytes as well as the interactions between them. By including the spontaneous adsorption of ions on graphene, our model can well support the experimental results, which strongly indicates the occurrence of such specific ion adsorption at the electrolyte-graphene interface.

**TABLE I.** Summary of the parameters for the calculation of  $V_{CNP}$  in NaCl, KCl, and HCl.

Electrolyte	$n_{imp} (\text{cm}^{-2})$	$sgn\left(\sigma_{ads}\right)$	$n_{ads}^{sat} (\text{cm}^{-2})$	$K_D$ (M)	$V_{fb}$ (V)
NaCl	$5 \times 10^{12}$	_	$5 \times 10^{13}$	0.004	0.08
KCl	$5 \times 10^{12}$	_	$5 \times 10^{13}$	0.004	0.06
HCl	$5 \times 10^{12}$	+	$5 \times 10^{13}$	0.05	0.06

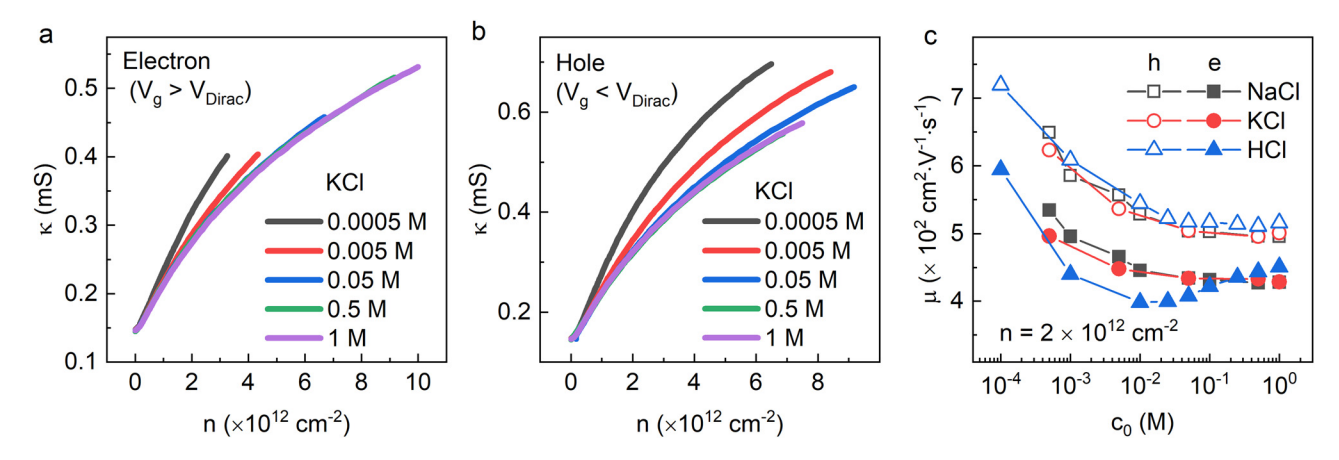


**FIG. 4.** The extracted conductivity  $\kappa$  as a function of the charge carrier density n of graphene in KCI for (a) electrons and (b) holes. (c) The extracted carrier mobility  $\mu$  as a function of the electrolyte concentration  $c_0$ . The alternative result of the electron mobility in HCl in (c) is caused by the gate current leakage due to hydrogen reduction at high  $V_g$  as can be observed in Fig. 2(c).

We further analyze the impact of the electrolytes on the charge carrier transport in graphene. When  $V_g$  is driven away from  $V_{CNP}$ , electrons/holes are injected into graphene, which would be compensated by the gain/loss of the ions at the interface according to the charge neutrality condition, i.e.,  $\Delta \sigma_{dl} = -\Delta \sigma_{gr}$ . By solving Eqs. (2) and (4), the carrier density n as a function of  $V_g$  can be derived, allowing us to extract the dependence of the conductivity  $\kappa$  on n from the  $I_d - V_g$  curves in Fig. 2. Figures 4(a) and 4(b) show the results measured for KCl. The curves exhibit an increasing sublinearity as n increases, and such a transition is enhanced as the concentration of the electrolytes increases. According to the self-consistent theory, 29,38-40 the carrier scattering in graphene on SiO2 is dominated by the charged impurities on SiO<sub>2</sub>, and such sublinearity is attributed to the spatial correlation effect between them. The enhancement of the sublinearity as the electrolyte concentration increases suggests a higher charge impurity density and/or an increased level of correlation among them. Since the charge impurities on SiO2 were protected by the graphene film, their density and spatial distribution are unchanged for all the measurements. Therefore, the origin of the increased charged impurities should be the adsorption of ions on the graphene surface, which would exhibit an intrinsically high correlation due to the electrostatic interaction between the ions. 41 Furthermore, as shown in Figs. 4(a) and 4(b), no further enhancement of sublinearity can be observed for  $c_0$  higher than 0.05 M, which suggests a saturation of ion species adsorbed on graphene at this concentration. According to the Langmuir adsorption isotherm [Eq. (7)], the density of the absorbed ions approaches saturation when the concentration reaches a few times the values of  $K_D$ . In this sense, the saturation of the sublinearity transition at  $c \ge 0.05$  M is in agreement with the previously assumed  $K_D$  of 0.004 M for Cl<sup>-</sup> adsorption on graphene. Figure 4(c) shows the extracted carrier mobility in graphene at  $n = 2 \times 10^{12} \,\mathrm{cm}^{-2}$  as a function of the electrolyte concentration. It is clear that the carrier mobility decreases as the concentration of the electrolytes increases, and such a decrease also approaches saturation for  $c_0 > K_D$ . The decrease in the carrier mobility indicates that extra scattering sources are introduced in the system, thus corroborating our hypothesis of adsorbed ions on the graphene surface.

In summary, we report the spontaneous adsorption of ions on graphene through an investigation of the electrolyte-graphene interface in the EGFET configuration. By incorporating a Langmuir-type adsorption term within the PB ionic theory, we show a quantitative alignment between the theoretical predictions and the experimentally measured with different electrolytes as a function of the ion concentrations. The adsorption of ions on graphene is further supported by analyzing the transport characteristics of these devices, which show enhanced sublinearity transition in the carrier density dependence of the conductivity and decreased carrier mobility as the electrolyte concentration increases. Since an accurate understanding of the chemico-physical interactions occurring at the electrolyte-graphene interface is critical for many applications of graphene, e.g., analytical chemistry, energy storage and conversion (e.g., fuels cells and batteries), water filtration, and biosensing, we expect our results to have profound implications in the field.

See the supplementary material for the details about the device fabrication, Raman characterization, and electrical measurement.

The experiments were performed at West Virginia University. We acknowledge the Shared Research Facilities at West Virginia University for device fabrication and material characterization. This work was supported by the U.S. National Science Foundation under Grant No. NSF1916894. L.C. acknowledges support from the Villum Fonden through the Young Investigator Program (Project No. 19130) and support from the Italian Ministry of Education, University and Research (MIUR) via "Programma per Giovani Ricercatori-Rita Levi Montalcini 2017." J.M.C. acknowledges support from Vinnova (Grant No. 2019-02878). J.E.S. was supported by the European Structural and Investment Funds in the FEDER component, through the Operational Competitiveness and Internationalization Programme (COMPETE 2020) (Project No. 39479; Funding Reference No.: POCI-01-0247-FEDER-39479) and by the Portuguese Foundation for Science and Technology (FCT) in the framework of the Strategic Funding No. UID/FIS/04650/2020.

## **DATA AVAILABILITY**

The data that support the findings of this study are available within this article.

### **REFERENCES**

- <sup>1</sup>H.-J. Butt, K. (Karlheinz) Graf, and M. Kappl, *Physics and Chemistry of Interfaces* (Wiley-VCH Verlag & Co. KGaA, Weinheim, 2003).
- <sup>2</sup>R. Sitko, B. Zawisza, and E. Malicka, TrAC Trends Anal. Chem. **51**, 33 (2013).
- <sup>3</sup>L. Bai, Y. Zhang, W. Tong, L. Sun, H. Huang, Q. An, N. Tian, and P. K. Chu, Electrochem. Energy Rev. 3, 395 (2020).
- <sup>4</sup>A. Boretti, S. Al-Zubaidy, M. Vaclavikova, M. Al-Abri, S. Castelletto, and S. Mikhalovsky, NPJ Clean Water 1, 5 (2018).
- <sup>5</sup>M. Pumera, Mater. Today **14**, 308 (2011).
- <sup>6</sup>F. Chen, J. Xia, D. K. Ferry, and N. Tao, Nano Lett. **9**, 2571 (2009).
- <sup>7</sup>C. Jang, S. Adam, J. H. Chen, E. D. Williams, S. D. Sarma, and M. S. Fuhrer, Phys. Rev. Lett. **101**, 146805 (2008).
- <sup>8</sup>A. K. M. Newaz, Y. S. Puzyrev, B. Wang, S. T. Pantelides, and K. I. Bolotin, Nat. Commun. 3, 734 (2012).
- <sup>9</sup>J. M. Caridad, G. Calogero, P. Pedrinazzi, J. E. Santos, A. Impellizzeri, T. Gunst, T. J. Booth, R. Sordan, P. Bøggild, and M. Brandbyge, Nano Lett. 18, 4675 (2018).
- <sup>10</sup>A. Ashraf, Y. Wu, M. C. Wang, K. Yong, T. Sun, Y. Jing, R. T. Haasch, N. R. Aluru, and S. Nam, Nano Lett. 16, 4708 (2016).
- <sup>11</sup>B. Radha, A. Esfandiar, F. C. Wang, A. P. Rooney, K. Gopinadhan, A. Keerthi, A. Mishchenko, A. Janardanan, P. Blake, L. Fumagalli, M. Lozada-Hidalgo, S. Garaj, S. J. Haigh, I. V. Grigorieva, H. A. Wu, and A. K. Geim, Nature 538, 222 (2016).
- <sup>12</sup>J. L. Xia, F. Chen, P. Wiktor, D. K. Ferry, and N. J. Tao, Nano Lett. 10, 5060 (2010).
- <sup>13</sup>F. Chen, J. Xia, and N. Tao, Nano Lett. **9**, 1621 (2009).
- <sup>14</sup>J. Xia, F. Chen, J. Li, and N. Tao, Nat. Nanotechnol. 4, 505 (2009).
- <sup>15</sup>I. Heller, S. Chatoor, J. Mä, M. A. G. Zevenbergen, C. Dekker, and S. G. Lemay, J. Am. Chem. Soc. **132**, 17149 (2010).
- <sup>16</sup>F. Chen, Q. Qing, J. Xia, J. Li, and N. Tao, J. Am. Chem. Soc. 131, 9908 (2009).
- <sup>17</sup>P. K. Ang, S. Wang, Q. Bao, J. T. L. Thong, and K. P. Loh, ACS Nano 3, 3587 (2009).

- <sup>18</sup>Z. L. Mišković and N. Upadhyaya, Nanoscale Res. Lett. 5, 505 (2010).
- <sup>19</sup>Z. L. Mišković, P. Sharma, and F. O. Goodman, Phys. Rev. B 86, 115437 (2012).
- <sup>20</sup>P. Sharma and Z. L. Mišković, J. Chem. Phys. **143**, 134118 (2015).
- <sup>21</sup>G. Shi, Y. Ding, and H. Fang, J. Comput. Chem. **33**, 1328 (2012).
- <sup>22</sup>D. J. Cole, P. K. Ang, and K. P. Loh, J. Phys. Chem. Lett. **2**, 1799 (2011).
- <sup>23</sup>C. D. Williams, J. Dix, A. Troisi, and P. Carbone, J. Phys. Chem. Lett. 8, 703 (2017).
- <sup>24</sup>L. Chen, Y. Guo, Z. Xu, and X. Yang, ChemPhysChem **19**, 2954 (2018).
- <sup>25</sup>G. Shi, J. Liu, C. Wang, B. Song, Y. Tu, J. Hu, and H. Fang, Sci. Rep. 3, 3436 (2013).
- <sup>26</sup>J. Dočkal, F. Moučka, and M. Lísal, J. Phys. Chem. C **123**, 26379 (2019).
- <sup>27</sup>D. L. McCaffrey, S. C. Nguyen, S. J. Cox, H. Weller, A. P. Alivisatos, P. L. Geissler, and R. J. Saykally, Proc. Natl. Acad. Sci. 114, 13369 (2017).
- <sup>28</sup>G. Shi, Y. Shen, J. Liu, C. Wang, Y. Wang, B. Song, J. Hu, and H. Fang, Sci. Rep. 4, 6793 (2014).
- <sup>29</sup>S. Adam, E. H. Hwang, V. M. Galitski, and S. D. Sarma, Proc. Natl. Acad. Sci. U. S. A. **104**, 18392 (2007).
- <sup>30</sup>C. Melios, C. E. Giusca, V. Panchal, and O. Kazakova, 2D Mater. 5, 022001 (2018)
- <sup>31</sup>M. S. Kilic, M. Z. Bazant, and A. Ajdari, Phys. Rev. E 75, 021502 (2007).
- <sup>32</sup>A. H. Castro Neto, F. Guinea, N. M. R. Peres, K. S. Novoselov, and A. K. Geim, Rev. Mod. Phys. 81, 109 (2009).
- 33P. Sharma and Z. L. Mišković, Phys. Rev. B 90, 125415 (2014).
- <sup>34</sup>M. Marino, L. Misuri, and D. Brogioli, arXiv:1403.3640 (2014).
- 35M. Kocman, M. Pykal, and P. Jurečka, Phys. Chem. Chem. Phys. 16, 3144 (2014).
- 36). D. Elliott, A. Troisi, and P. Carbone, J. Chem. Theory Comput. 16, 5253 (2020).
- <sup>37</sup>L. Shi, A. Xu, G. Chen, and T. Zhao, J. Phys. Chem. Lett. **8**, 4354 (2017).
- <sup>38</sup>Q. Li, E. H. Hwang, E. Rossi, and S. D. Sarma, Phys. Rev. Lett. **107**, 156601
- <sup>39</sup>J. Yan and M. S. Fuhrer, Phys. Rev. Lett. **107**, 206601 (2011).
- <sup>40</sup>P. Pedrinazzi, J. M. Caridad, D. M. A. Mackenzie, F. Pizzocchero, L. Gammelgaard, B. S. Jessen, R. Sordan, T. J. Booth, and P. Bøggild, Appl. Phys. Lett. 112, 033101 (2018).
- <sup>41</sup>J. B. Allen and R. F. Larry, *Electrochemical Methods: Fundamentals and Applications*, 2nd ed. (John Wiley & Sons, Inc., New York, NY, 2001).